Regulation of Cell–Cell Adhesion by Rac and Rho Small G Proteins in MDCK Cells

Kenji Takaishi,* Takuya Sasaki,* Hirokazu Kotani,* Hideo Nishioka,‡ and Yoshimi Takai*‡

*Department of Molecular Biology and Biochemistry, Osaka University Medical School, Suita 565, Japan; and ‡Takai Biotimer Project, ERATO, Japan Science and Technology Corporation, JCR Pharmaceuticals Co., Ltd., Nishi-ku, Kobe 651-22, Japan

Abstract. The Rho small G protein family, consisting of the Rho, Rac, and Cdc42 subfamilies, regulates various cell functions, such as cell shape change, cell motility, and cytokinesis, through reorganization of the actin cytoskeleton. We show here that the Rac and Rho subfamilies furthermore regulate cell–cell adhesion. We prepared MDCK cell lines stably expressing each of dominant active mutants of RhoA (sMDCK-RhoDA), Rac1 (sMDCK-RacDA), and Cdc42 (sMDCK-Cdc42DA) and dominant negative mutants of Rac1 (sMDCK-RacDN) and Cdc42 (sMDCK-Cdc42DN) and analyzed cell adhesion in these cell lines. The actin filaments at the cell–cell adhesion sites markedly increased in sMDCK-RacDA cells, whereas they apparently decreased in sMDCK-RacDN cells, compared with those in wild-type MDCK cells. Both E-cadherin and β-catenin, adherens junctional proteins, at the cell–cell adhesion sites also increased in sMDCK-RacDA cells, whereas both of them decreased in sMDCK-RacDN cells. The detergent solubility assay indicated that the amount of detergent-insoluble E-cadherin increased in sMDCK-RacDA cells, whereas it slightly decreased in sMDCK-RacDN cells, compared with that in wild-type MDCK cells. In sMDCK-RhoDA, -Cdc42DA, and -Cdc42DN cells, neither of these proteins at the cell–cell adhesion sites was apparently affected. ZO-1, a tight junctional protein, was not apparently affected in any of the transformant cell lines. Electron microscopic analysis revealed that sMDCK-RacDA cells tightly made contact with each other throughout the lateral membranes, whereas wild-type MDCK and sMDCK-RacDN cells tightly and linearly made contact at the apical area of the lateral membranes. These results suggest that the Rac subfamily regulates the formation of the cadherin-based cell–cell adhesion. Microinjection of C3 into wild-type MDCK cells inhibited the formation of both the cadherin-based cell–cell adhesion and the tight junction, but microinjection of C3 into sMDCK-RacDA cells showed little effect on the localization of the actin filaments and E-cadherin at the cell–cell adhesion sites. These results suggest that the Rho subfamily is necessary for the formation of both the cadherin-based cell–cell adhesion and the tight junction, but not essential for the Rac subfamily-regulated, cadherin-based cell–cell adhesion.

The Rho family belongs to the small G protein superfamily and consists of the Rho, Rac, and Cdc42 subfamilies (for reviews see Hall, 1994; Takai et al., 1995). The Rho subfamily, consisting of three members, RhoA, -B, and -C, regulates a wide variety of cell functions, such as cell shape change (Rubin et al., 1988; Chardin et al., 1989; Paterson et al., 1990; Miura et al., 1993), formation of stress fibers and focal adhesions (Paterson et al., 1990; Ridley and Hall, 1992, 1994; Self et al., 1993; Ridley et al., 1995), cell motility (Stasia et al., 1991; Takaishi et al., 1993, 1994), platelet aggregation (Morii et al., 1992), smooth muscle contraction (Hirata et al., 1992), lymphocyte toxicity (Lang et al., 1992), cytokinesis (Kishi et al., 1993; Mabuchi et al., 1993), lymphocyte aggregation (Tominaga et al., 1993), neurite retraction (Jalink et al., 1994), formation of tight junction and perijunctional actin (Nusrat et al., 1995), endocytosis (Schmalzing et al., 1995; Lamaze et al., 1996), and exocytosis (Komuro et al., 1996). The Rac subfamily, consisting of two members, Rac1 and -2, regulates formation of lamellipodia and membrane ruffles (Ridley et al., 1992), NADPH oxidase-catalyzed superoxide formation (Abo et al., 1991; Knaus et al., 1991; Ando et al., 1992; Mizuno et al., 1992), endocytosis (Lamaze et al., 1996), and exocytosis (Komuro et al., 1996; O'Sullivan et al.,

Address all correspondence to Y. Takai, Department of Molecular Biology and Biochemistry, Osaka University Medical School, Suita 565, Japan. Tel.: (81) 6 879 3401. Fax: (81) 6 879 3419. E-mail: ytakai@molbio.med.osaka-u.ac.jp

Hirokazu Kotani's present address is First Department of Internal Medicine, Mie Univeristy School of Medicine, 2-174 Edobashi, Tsu, Mie 514, Japan.

1996). The Cdc42 subfamily, consisting of one member, regulates formation of filopodia (Kozma et al., 1995; Nobes and Hall, 1995) and adhesion of helper T cells towards antigen-presenting cells (Stowers et al., 1995).

Most of these cell functions are closely related to the cytoskeleton system, particularly the actin cytoskeleton. The actin cytoskeleton is known to play an important role also in cell–cell adhesion. In epithelial cells, cells are linked together by a junctional complex comprised of adherens junctions, tight junctions, and desmosomes. Adherens and tight junctions are linked to actin filaments, whereas desmosomes are linked to intermediate filaments (for reviews see Madara, 1988; Tsukita et al., 1992, 1993). Cadherins, constituting a family of transmembrane proteins that interact with each other at the extracellular surface, are localized at adherens junctions, and are responsible for Ca^{2+}-dependent cell–cell adhesion (for reviews see Tsukita et al., 1992; Takeichi, 1995). Cadherins are associated with several cytoplasmic proteins, such as α-, β-, and γ-catenin (plakoglobin) and p120 (Vestweber and Kemler, 1984; Peyrieras et al., 1985; Ozawa et al., 1989; Shibamoto et al., 1995). As to the regulatory mechanism of cadherins, the tyrosine phosphorylation of β-catenin is associated with dysfunction of cadherins (Matsuyoshi et al., 1992; Behrens et al., 1993; Hamaguchi et al., 1993). APC competes for the interaction of cadherins with β-catenin (Hülsken et al., 1994). However, the regulatory mechanism of the cadherin-based cell–cell adhesion is not fully understood, and the molecular mechanism of the linkage between cadherins and actin filaments also remains to be clarified. Occludins, transmembrane proteins that interact with each other at the extracellular surface, are localized at tight junctions (Furuse et al., 1993). The occludin cytoplasmic tail interacts with the cytoplasmic plaque proteins, ZO-1 and -2 (Woods and Bryant, 1993; Furuse et al., 1994; Jesaitis and Goodenough, 1994). In addition, several proteins, including cingulin (Citi et al., 1988), the 7H6 antigen (Zhong et al., 1993), Rab13 small G protein (Zahraoui et al., 1994), and symplekin (Keon et al., 1996) are localized at tight junctions. As to the regulatory mechanism of the formation of tight junctions, the intercellular binding of cadherins triggers the formation of adherens junctions, followed by the formation of tight junctions in the Ca^{2+}-induced formation of cell–cell adhesion (Gonzalez-Mariscal et al., 1985, 1990; Contreras et al., 1992). Activation of protein kinase C (PKC)[1] induces the formation of tight junctions without the formation of adherens junctions in epithelial cells cultured in a low Ca^{2+} medium (Balda et al., 1993). However, the regulatory mechanism of the formation of tight junctions is not fully understood, and the molecular mechanism of the linkage between occludin and actin filaments also remains to be clarified.

As to the regulation of cell–cell adhesion by the Rho family, the Rho subfamily regulates the formation of the tight junction in polarized epithelial cells (Nusrat et al., 1995). Moreover, the *Drosophila* Rac subfamily regulates actin assembly at the adherens junctions of the wing disc epithelium (Luo et al., 1994; Eaton et al., 1995). However, it has not been studied whether the mammalian Rho family regulates the formation of the cadherin-based cell–cell adhesion. Here we attempted to address this issue using MDCK cell lines stably expressing various mutants of the Rho family members.

1. *Abbreviations used in this paper*: ERM, Ezrin, Radixin, Moesin; GEP, GDP/GTP exchange protein; PKC, protein kinase C; TPA, 12-*O*-tetradecanoylphorbol-13-acetate.

Materials and Methods

Materials and Chemicals

MDCK cells were supplied by W. Birchmeier (Max-Delbruck-Center for Molecular Medicine, Berlin, Germany). The cDNA of RhoA was provided by P. Madaule (Kyoto University, Kyoto, Japan). The cDNAs of V12Rac1, with a mutation of amino acid 12 from Gly to Val, and N17Rac1, with a mutation of amino acid 17 from Thr to Asn, were provided by A. Hall (University College London, London, England). The cDNA of Cdc42 was provided by P. Polakis (Onyx Pharmaceuticals, Richmond, CA). Mutagenesis of Gly to Val at codon 14 of RhoA (V14RhoA), Gly to Val at codon 12 of Cdc42 (V12Cdc42), or Thr to Asn at codon 17 of Cdc42 (N17Cdc42) was carried out by site-directed mutagenesis. The pSRαneo expression plasmid was donated from A. Miyajima (Tokyo University, Tokyo, Japan). C3 was supplied by S. Narumiya (Kyoto University, Kyoto, Japan). The C3 sample for the microinjection experiments was prepared as described (Kotani et al., 1997). Hybridoma cells expressing the anti-*myc* mouse mAb (9E10) were purchased from American Type Culture Collection (Rockville, MD). The anti–E-cadherin rat mAb (ECCD-2) and mouse mAb (C20820) were obtained from TAKARA Shuzo, Inc. (Shiga, Japan) and Transduction Laboratories, Inc. (Lexington, KY), respectively. The anti–β-catenin mouse mAb (5H10) and the anti–ZO-1 mouse mAb were supplied by M.J. Wheelock (University of Toledo, Toledo, Ohio) and Sh. Tsukita (Kyoto University, Kyoto, Japan), respectively. The anti-IQGAP rabbit polyclonal antibody was supplied by K. Kaibuchi (Nara Institute of Science and Technology, Ikoma, Japan). Rhodamine-phalloidin was purchased from Molecular Probes, Inc. (Eugene, OR). Secondary antibodies for immunofluorescence microscopy were obtained from Chemicon International, Inc. (Temecula, CA). Other materials and chemicals were obtained from commercial sources.

Construction of Expression Plasmids of Rho, Rac, and Cdc42 Mutants

The pSRα-*myc*–tagged V14RhoA (*myc*-V14RhoA), pSRα-*myc*–tagged V12Rac1 (*myc*-V12Rac1), pSRα-*myc*–tagged N17Rac1 (*myc*-N17Rac1), pSRα-*myc*–tagged V12Cdc42 (*myc*-V12Cdc42), and pSRα-*myc*–tagged N17Cdc42 (*myc*-N17Cdc42) expression plasmids were constructed as described (Takaishi et al., 1995). Briefly, the pSRαneo plasmid was cut at the XhoI and BamHI sites and ligated to a double-stranded oligonucleotide encoding the peptide sequence, MEQKLISEEDL, which is the epitope of the 9E10 anti-*myc* mAb to generate the pSRα-*myc* plasmid. The 0.6-kb fragments containing full length V14RhoA, V12Rac1, N17Rac1, V12Cdc42, and N17Cdc42 coding sequences with the BamHI site upstream of the initiation methionine codon and downstream of the termination codon were synthesized by PCR. These fragments were digested by BamHI and ligated into the BamHI site of the pSRα-*myc* plasmid.

Cell Culture, Transfection, and Microinjection

MDCK cells were maintained at 37°C in a humidified atmosphere of 10% CO_2 and 90% air in DME containing 10% FCS (GIBCO BRL, Grand Island, NY), penicillin (100 U/ml), and streptomycin (100 μg/ml). Transfection of pSRα-*myc*–V14RhoA, -V12Rac1, -N17Rac1, -V12Cdc42, or -N17Cdc42 was carried out using the calcium phosphate coprecipitation method, and cell clones were isolated by resistance to G418. For the Ca^{2+}-switch experiments, the cells were cultured in serum-free DME and 5 mM EGTA (low Ca^{2+} DME) for 2 h. They were then transferred to serum-free DME (normal Ca^{2+} DME). MDCK cells for the microinjection experiments were seeded at a density of 3×10^4 cells/dish onto 35-mm grid dishes. 2 d after seeding, C3 was comicroinjected with 5 mg/ml of rabbit IgG into the cells as described (Kotani et al., 1997).

Immunoblotting and Immunoprecipitation

myc-Tagged proteins, E-cadherin, and β-catenin in MDCK cells were

detected by immunoblotting with the 9E10, C20820, and 5H10 mAbs, respectively. For detection of *myc*-tagged proteins, subconfluent monolayers of MDCK cells were lysed in Lysis Buffer A (20 mM Tris/HCl, pH 7.4, containing 150 mM NaCl, 10 mM $MgCl_2$, 1% NP-40, and 100 μM *p*-amidinophenyl methanesulfonyl fluoride) and sonicated. For detection of E-cadherin and β-catenin, the cells were lysed in Lysis Buffer B (Hepes-buffered saline [HCMF; Takeichi, 1977] containing 1 mM $CaCl_2$, 1% NP-40, 100 μM *p*-amidinophenyl methanesulfonyl fluoride, and 20 μg/ml leupeptin) and sonicated. 50 μg of each protein sample from the homogenates was subjected to SDS-PAGE, and the separated proteins were electrophoretically transferred to a nitrocellulose membrane sheet. The sheet was processed to detect *myc*-tagged proteins with the 9E10 mAb, E-cadherin with the C20820 mAb, and β-catenin with the 5H10 mAb as a primary antibody, using the ECL detection kit (Amersham Corp., Arlington Heights, IL). For immunoprecipitation of *myc*-tagged proteins with the 9E10 mAb, the homogenates lysed in Lysis Buffer A were clarified by centrifugation at 12,000 *g* for 10 min, and the supernatants were immunoprecipitated with the 9E10 mAb crosslinked to protein A–Sepharose 4B using dimethyl pimelimidate. The immunoprecipitates were boiled with SDS-sample buffer. *myc*-Tagged proteins in the immunoprecipitates were detected by immunoblotting with the 9E10 mAb as described above.

Detergent Extraction of E-Cadherin

Detergent extraction of E-cadherin from MDCK cells was performed as described (Nagafuchi and Takeichi, 1988) with slight modifications. Briefly, subconfluent monolayers of MDCK cells grown on 6-cm dishes were washed with HCMF containing 1 mM $CaCl_2$ (HMF; Takeichi, 1977), collected by scraping with a rubber policeman, and then centrifuged at 5,000 *g* for 1 min. After the supernatant was removed, 200 μl of various concentrations (0–0.5%) of NP-40 in HMF were added. The samples were incubated for 10 min with mild pipetting and then centrifuged at 100,000 *g* for 30 min. To the supernatant, 100 μl of 3× SDS-sample buffer was added and used as the detergent-soluble fraction. The pellet fraction was dissolved in 300 μl of 1× SDS-sample buffer and used as the detergent-insoluble fraction. E-Cadherin was detected by immunoblotting with the C20820 mAb.

Immunofluorescence Microscopy

For localization of actin filaments, *myc*-tagged proteins, and ZO-1, immunofluorescence microscopy was performed as described (Kotani et al., 1997). Briefly, cells were fixed in 3.7% paraformaldehyde in PBS for 20 min. The fixed cells were incubated with 50 mM NH_4Cl in PBS for 10 min and permeabilized with PBS containing 0.2% Triton X-100 for 10 min. After being soaked in 10% FCS/PBS for 30 min, the cells were treated with the first antibody in 10% FCS/PBS for 1 h. The cells were then washed with PBS three times, followed by incubation with the second antibody in 10% FCS/PBS for 1 h. For the detection of actin filaments, rhodamine-phalloidin was mixed with the second antibody solution. After being washed with PBS three times, the cells were examined using a confocal laser scanning microscope (LSM 410; Carl Zeiss, Oberkochen, Germany). For localization of E-cadherin and β-catenin, cells were fixed in 3.7% paraformaldehyde in HMF for 20 min, followed by the same procedures as described above.

Electron Microscopy

Cells cultured on the poly-L-lysine–coated celldesk LF1 (Sumitomo Bake, Akita, Japan) were fixed with 2.5% glutaraldehyde in PBS for 2 h, followed by postfixation with 1% OsO_4 in 0.1 M cacodylate-HCl, pH 7.4, for 1 h. The samples were dehydrated in a graded series of ethanol, embedded in Epon812, and examined using an electron microscope (H-7100; Hitachi, Tokyo, Japan).

Immunoelectron microscopy using the silver enhancement technique was done as described (Mizoguchi et al., 1994). Briefly, cells cultured on the poly-L-lysine–coated celldesk LF1 were fixed with 4% paraformaldehyde in PBS. The samples were incubated with the ECCD-2 anti–E-cadherin mAb or the 5H10 anti–β-catenin mAb followed by incubation with an anti–rat IgG antibody or an anti–mouse IgG antibody, respectively, coupled with 1.4-nm gold particles (Nanoprobes Inc., Stony Brook, NY). After being washed, the samples were fixed with 1% glutaraldehyde in PBS for 10 min, and the sample-bound gold particles were silver enhanced by the HQ-silver kit (Nanoprobes Inc.) at 18°C for 8 min. The samples were again washed and postfixed with 0.8% OsO_4 in 0.1 M cacodylate-HCl, pH 7.4, for 1 h. The samples were dehydrated in a graded series of ethanol, embedded in Epon812, and examined using an electron microscope (JEM-1200EX; JEOL, Tokyo, Japan).

Results

Preparation of MDCK Cell Lines Stably Expressing Various Rho, Rac, and Cdc42 Mutants

The pSRαneo expression plasmid, containing each of the cDNAs of *myc*-V14RhoA, a dominant active mutant of RhoA, *myc*-V12Rac1, a dominant active mutant of Rac1, *myc*-N17Rac1, a dominant negative mutant of Rac1, *myc*-V12Cdc42, a dominant active mutant of Cdc42, and *myc*-N17Cdc42, a dominant negative mutant of Cdc42, was transfected into MDCK cells, and cell clones were isolated by resistance to G418. Three clones expressing *myc*-V14RhoA (sMDCK-RhoDA), four clones expressing *myc*-V12Rac1 (sMDCK-RacDA), two clones expressing *myc*-N17Rac1 (sMDCK-RacDN), two clones expressing *myc*-V12Cdc42 (sMDCK-Cdc42DA), and four clones expressing *myc*-N17Cdc42 (sMDCK-Cdc42DN) were obtained. *myc*-V14RhoA in sMDCK-RhoDA cell line clone 5 (sMDCK-RhoDA-5) and *myc*-V12Rac1 in sMDCK-RacDA cell line clone 1 (sMDCK-RacDA-1) were undetectable by immunoblotting with the anti-*myc* Ab using the cell lysates (Fig. 1 *a*, lanes *2* and *3*), but the proteins were detected in the immunoprecipitated samples from the cell lysates (Fig. 1 *b*, lanes *2* and *3*). *myc*-N17Rac1 in the sMDCK-RacDN cell line clone 2 (sMDCK-RacDN-2), *myc*-V12Cdc42 in the sMDCK-Cdc42DA cell line clone 2 (sMDCK-Cdc42DA-2), and *myc*-N17Cdc42 in the sMDCK-Cdc42DN cell line clone 6 (sMDCK-Cdc42DN-6) were detected in both the cell lysates and the immunoprecipitated samples (Fig. 1, *a* and *b*, lanes *4–6*). The expression level of *myc*-V14RhoA was calculated to be less than one tenth of endogenous RhoA in sMDCK-RhoDA-5 when the expression level of endogenous RhoA was estimated by immunoblotting with the anti-RhoA polyclonal antibody (data not shown). Because any anti-Rac1 Ab or anti-Cdc42 Ab is not currently available, we could not compare the expression levels of Rac1 and Cdc42 mutants with those of endogenous Rac1 and Cdc42 in sMDCK-RacDA-1, -RacDN-2, -Cdc42DA-2, and -Cdc42DN-6 cells, respectively.

myc-V14RhoA and -V12Rac1 were also detected in the immunoprecipitated samples from the cell lysates of all the other clones of sMDCK-RhoDA and -RacDA, although they were not detected directly from the cell lysates (data not shown). The reason why cell clones expressing high levels of both *myc*-V14RhoA and -V12Rac1 could not be obtained is not known. However, because the expression of a dominant active or negative mutant of Rho1p causes lethality to the cells in the yeast *Saccharomyces cerevisiae* (Tanaka, K., and Y. Takai, unpublished observations). Therefore, these proteins at higher expression levels may cause lethality to the cells. *myc*-N17Rac1 was detected from the cell lysates of the other clone of sMDCK-RacDN, and the expression level of *myc*-N17Rac1 in this clone was similar to that in sMDCK-RacDN-2 (data not shown). *myc*-V12Cdc42 was detected in the immunoprecipitated samples from the cell lysates of the other clone of sMDCK-Cdc42DA, but it was not detected directly from

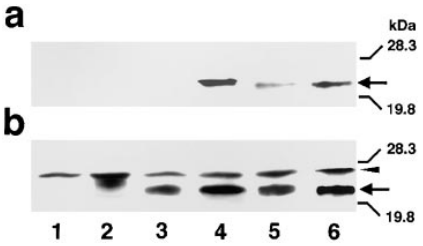

Figure 1. Expression of various Rho, Rac, and Cdc42 mutants in stable transformants of MDCK cell lines. Subconfluent MDCK cells were lysed and protein samples were directly subjected to SDS-PAGE (13% polyacrylamide). The separated proteins were processed for immunoblotting with the 9E10 anti-*myc* mAb (*a*). Subconfluent MDCK cells were lysed, and protein samples were immunoprecipitated with the 9E10 anti-*myc* mAb crosslinked to protein A-Sepharose 4B. The immunoprecipitates were subjected to SDS-PAGE (13% polyacrylamide) and the separated proteins were processed for immunoblotting with the 9E10 mAb (*b*). lane *1*, Wild-type MDCK cell line; lane *2*, sMDCK-RhoDA-5 cell line expressing *myc*-V14RhoA; lane *3*, sMDCK-RacDA-1 cell line expressing *myc*-V12Rac1; lane *4*, sMDCK-RacDN-2 cell line expressing *myc*-N17Rac1; lane *5*, sMDCK-Cdc42DA-2 cell line expressing *myc*-V12Cdc42; lane *6*, sMDCK-Cdc42DN-6 cell line expressing *myc*-N17Cdc42. Arrows indicate *myc*-tagged proteins. The mobility of *myc*-V14RhoA was slightly slower than that of *myc*-V12Rac1, -N17Rac1, -V12Cdc42, and -N17Cdc42. An arrowhead indicates the light chain of the 9E10 anti-*myc* mAb, which was detected because a part of the light chain of the 9E10 anti-*myc* mAb crosslinking to protein A-sepharose 4B was detached from the beads by boiling in SDS-sample buffer. The prestained protein markers used were soybean trypsin inhibitor (molecular weight, 28,300) and lysozyme (molecular weight, 19,800).

the cell lysates, indicating that the expression level of *myc*-V12Cdc42 was less than that in sMDCK-Cdc42DA-2 cells (data not shown). *myc*-N17Cdc42 was detected in both the cell lysates and the immunoprecipitated samples of all the other clones of sMDCK-Cdc42DN, although the expression levels of *myc*-N17Cdc42 varied among these clones (data not shown).

Localization of the Actin Cytoskeleton and Cell Shape in MDCK Cell Lines Stably Expressing Various Rho, Rac, and Cdc42 Mutants

We first analyzed the localization of the actin cytoskeleton by staining with rhodamine-phalloidin in wild-type and transformant cell lines. Confocal microscopic images at the basal levels showed that weak formation of stress fibers and weak localization of actin filaments at the cell–cell adhesion sites were observed in wild-type MDCK, sMDCK-RacDN-2, -Cdc42DA-2, and -Cdc42DN-6 cells, whereas prominent stress fibers were observed in sMDCK-RhoDA-5 cells (Fig. 2, *a*, *b*, and *d–f*). sMDCK-RacDA-1 cells possessed weak stress fibers like wild-type MDCK cells, but the actin filaments at the cell–cell adhesion sites markedly increased in sMDCK-RacDA-1 cells (Fig. 2 *c*). Confocal microscopic images at the apical, junctional levels showed that actin filaments were localized at the cell–cell adhesion sites in wild-type MDCK, sMDCK-RhoDA-5, -Cdc42DA-2, and -Cdc42DN-6 cells to a similar degree (Fig. 2, *g*, *h*, *k*, and *l*), whereas sMDCK-RacDA-1 cells possessed denser

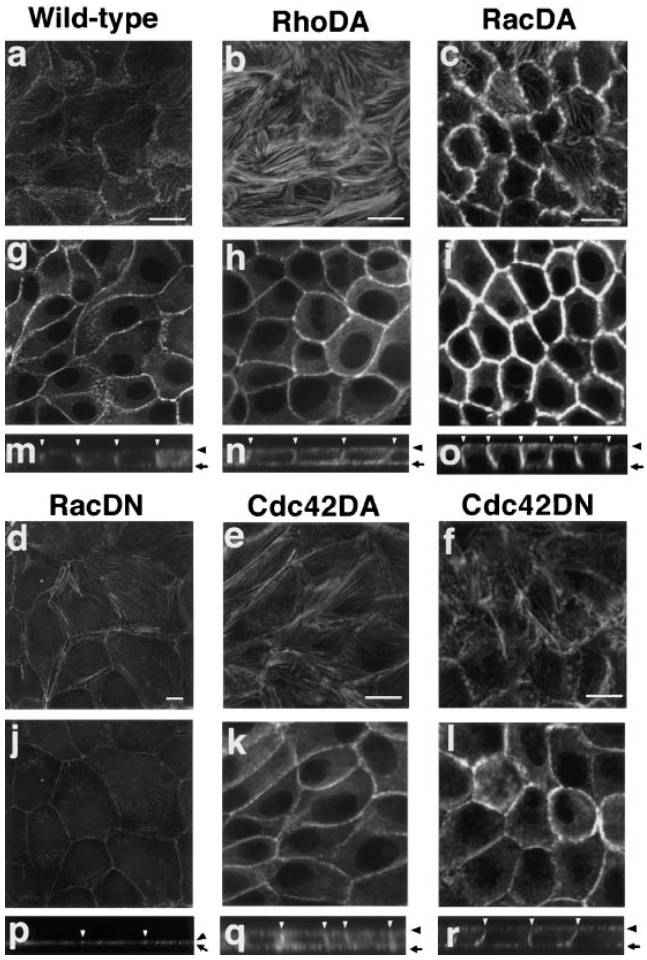

Figure 2. Localization of the actin cytoskeleton and cell shape in MDCK cells stably expressing various Rho, Rac, and Cdc42 mutants. Wild-type MDCK cells (*a*, *g*, and *m*), sMDCK-RhoDA-5 cells (*b*, *h*, and *n*), sMDCK-RacDA-1 cells (*c*, *i*, and *o*), sMDCK-RacDN-2 cells (*d*, *j*, and *p*), sMDCK-Cdc42DA-2 cells (*e*, *k*, and *q*), and sMDCK-Cdc42DN-6 cells (*f*, *l*, and *r*) were stained with rhodamine-phalloidin and analyzed by confocal microscopy. (*a–f*) Basal levels; (*g–l*) apical, junctional levels; (*m–r*) vertical sections. White arrowheads indicate the cell–cell adhesion sites. Black arrowheads and arrows indicate the apical and basal levels of the cells, respectively. Note that the scale in RacDN panels (*d*, *j*, and *p*) is different from those in the other panels. The results shown are representative of three independent experiments. Bars, 10 μm.

and thicker actin filaments at the cell–cell adhesion sites than the other cell lines, and sMDCK-RacDN-2 cells possessed weaker and less distinct actin filaments at the same area (Fig. 2, *i* and *j*). These changes of the actin filaments at the cell–cell adhesion sites were also visualized in the vertical sections (Fig. 2, *m–r*). The actin filaments at the cell–cell adhesion sites were observed at the lateral membranes in wild-type MDCK cells, and they tended to be more condensed at the apical regions (Fig. 2 *m*). The staining pattern of the actin filaments at the cell–cell adhesion sites in sMDCK-RhoDA-5, -Cdc42DA-2, and -Cdc42DN-6 cells resembled that in wild-type MDCK cells (Fig. 2, *n*, *q*, and *r*). However, in sMDCK-RacDA-1 cells, the staining of the actin filaments at the cell–cell adhesion sites was dense

and thick, and the increased staining was observed throughout the lateral membranes (Fig. 2 *o*). In contrast, the staining of the actin filaments at the cell–cell adhesion sites became weaker and more indistinct in sMDCK-RacDN-2 cells (Fig. 2 *p*). The changes in the actin cytoskeleton observed in sMDCK-RhoDA-5, -RacDA-1, -RacDN-2, -Cdc42DA-2, and -Cdc42DN-6 cells were similarly observed in all the other clones stably expressing V14RhoA, V12Rac1, N17Rac1, V12Cdc42, and N17Cdc42, respectively (data not shown). We have previously obtained an MDCK cell line transfected with the pSRα-*myc* vector alone (cMDCK; Takaishi et al., 1995), and the staining pattern of the actin filaments at the cell–cell adhesion sites in cMDCK cells was similar to that in wild-type MDCK cells (data not shown). These results indicate that the Rac subfamily regulates the formation of the actin filaments at the cell–cell adhesion sites, whereas the Rho subfamily regulates the formation of stress fibers.

The shapes of sMDCK-RacDA-1 and -RacDN-2 cells were different from those of the other cell lines. sMDCK-RacDA-1 cells were slightly thicker, and sMDCK-RacDN-2 cells were thinner than the other cell lines (Fig. 2, *m–r*). Moreover, the diameter of sMDCK-RacDN-2 cells was apparently larger than those of the other cell lines (Fig. 2, *m–r*). The essentially same results were obtained in the other cell lines stably expressing V14RhoA, V12Rac1, N17Rac1, V12Cdc42, or N17Cdc42 (data not shown). These results indicate that the Rac subfamily furthermore affects the cell shape of MDCK cells.

Localization of E-Cadherin, β-Catenin, and ZO-1 in MDCK Cell Lines Stably Expressing Various Rho, Rac, and Cdc42 Mutants

Because markedly different localization patterns of actin filaments were observed at the cell–cell adhesion sites of sMDCK-RacDA and -RacDN cells, compared with those of the other cell lines, as described above, we next investigated the localization of E-cadherin and β-catenin, both of which are the structural proteins of adherens junction (for reviews see Tsukita et al., 1992; Takeichi, 1995), in these cell lines. The staining of E-cadherin at the junctional levels in sMDCK-RhoDA-5 cells was similar to that in wild-type MDCK cells (Fig. 3, *a* and *b*). The staining of E-cadherin was apparently denser and thicker in sMDCK-RacDA-1 cells but weaker in sMDCK-RacDN-2 cells (Fig. 3, *c* and *d*). The staining of E-cadherin at the area of about apical two thirds of the lateral membranes was relatively stronger than that at the area of about basal one third of the lateral membranes in wild-type MDCK and sMDCK-RhoDA-5 cells (Fig. 3, *e* and *f*). However, the staining of E-cadherin increased at all of the lateral membranes in sMDCK-RacDA-1 cells (Fig. 3 *g*), whereas it was weak throughout the lateral membranes in sMDCK-RacDN-2 cells (Fig. 3 *h*). The staining patterns of β-catenin were essentially similar to those of E-cadherin in wild-type MDCK, sMDCK-RhoDA-5, -RacDA-1, and -RacDN-2 cells (Fig. 3, *i–p*). These staining patterns of both E-cadherin and β-catenin were essentially similar to those of the actin filaments at the cell–cell adhesion sites. The essentially same results were obtained when E-cadherin and β-catenin were stained in the other MDCK cell lines stably expressing V14RhoA, V12Rac1, or N17Rac1 (data not shown). The stainings of both E-cadherin and β-catenin at the junctional levels in all the clones of both sMDCK-Cdc42DA and -Cdc42DN were similar to those in wild-type MDCK cells (data not shown). These results indicate that the Rac subfamily regulates not only the formation of the actin filaments but also the localization of E-cadherin and β-catenin at the cell–cell adhesion sites in MDCK cells.

Consistent with the results obtained by immunofluorescence microscopy, the detergent solubility assay indicated

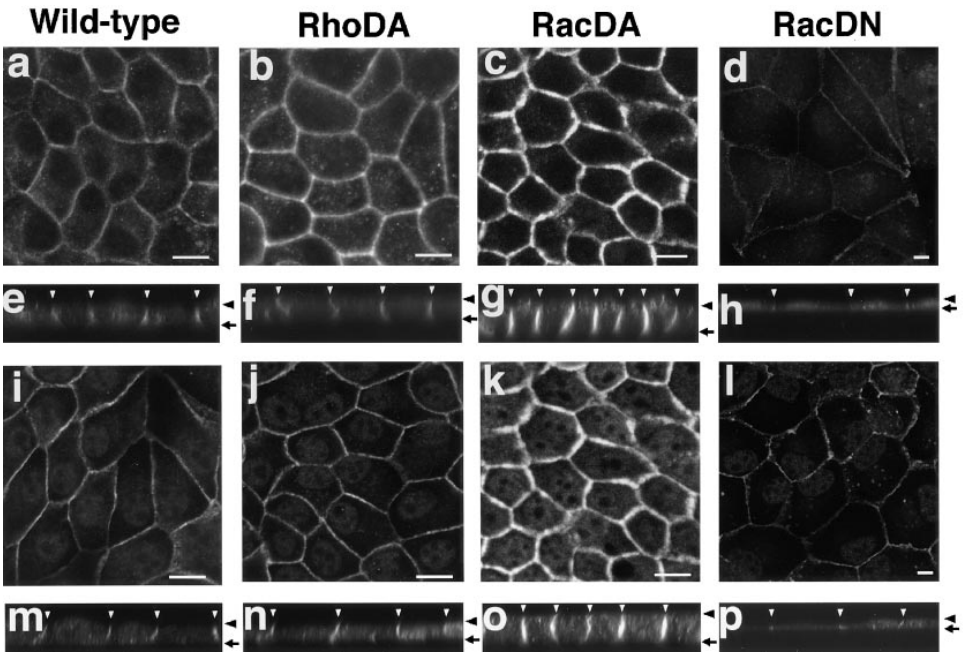

Figure 3. Localization of E-cadherin and β-catenin in sMDCK-RhoDA-5, -RacDA-1, and -RacDN-2 cells. Wild-type MDCK cells (*a*, *e*, *i*, and *m*), sMDCK-RhoDA-5 cells (*b*, *f*, *j*, and *n*), sMDCK-RacDA-1 cells (*c*, *g*, *k*, and *o*), and sMDCK-RacDN-2 cells (*d*, *h*, *l*, and *p*) were stained with the ECCD-2 anti–E-cadherin mAb (*a–h*) or the 5H10 anti–β-catenin mAb (*i–p*) and analyzed by confocal microscopy. (*a–d* and *i–l*) Junctional levels; (*e–h* and *m–p*) vertical sections. White arrowheads indicate the cell–cell adhesion sites. Black arrowheads and arrows indicate the apical and basal levels of the cells, respectively. Note that the scales in RacDN panels (*d*, *h*, *l*, and *p*) are different from those in the other panels. The results shown are representative of three independent experiments. Bars, 10 μm.

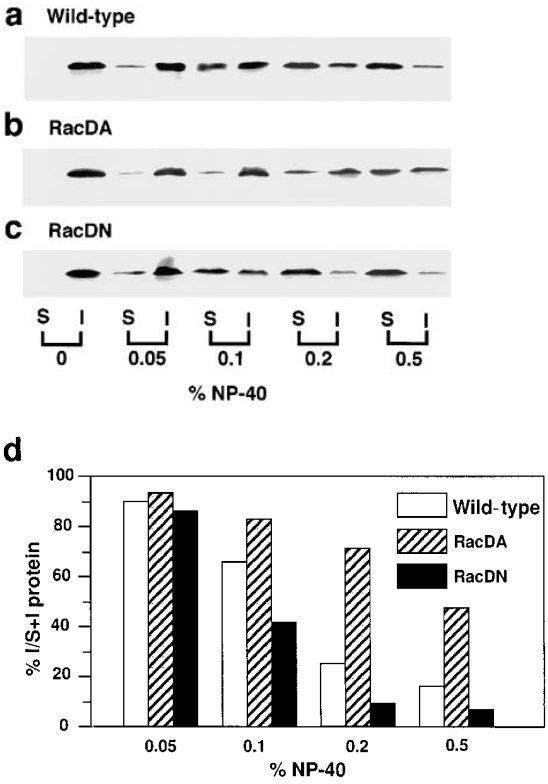

Figure 4. Detergent solubility of E-cadherin from wild-type MDCK, sMDCK-RacDA-1, and -RacDN-2 cells. Wild-type MDCK (*a*), sMDCK-RacDA-1 (*b*), and sMDCK-RacDN-2 cells (*c*) were incubated with various concentrations of NP-40, and the amounts of E-cadherin in the detergent-soluble (*S*) and -insoluble (*I*) fractions were measured by immunoblotting with the C20820 anti–E-cadherin mAb. *d* shows the amount of the insoluble E-cadherin as a percentage of the amount of total E-cadherin, i.e., S plus I, by estimation using densitometer.

that the amount of the actin cytoskeleton-associated E-cadherin increased in sMDCK-RacDA-1 cells, whereas it decreased in sMDCK-RacDN-2 cells. Wild-type MDCK, sMDCK-RacDA-1, and -RacDN-2 cells were incubated with various concentrations of NP-40, and the amounts of E-cadherin in the detergent-soluble and -insoluble fractions were measured by immunoblotting. The amount of E-cadherin remaining in the insoluble fraction increased in sMDCK-RacDA-1 cells and decreased in sMDCK-RacDN-2 cells, compared with that in wild-type MDCK cells (Fig. 4). About 15, 50, and 7% of E-cadherin was insoluble in the presence of 0.5% NP-40 in wild-type MDCK, sMDCK-RacDA-1, and -RacDN-2 cells, respectively.

We confirmed by immunoblotting that the expression levels of E-cadherin and β-catenin were not markedly different among wild-type, sMDCK-RhoDA-5, -RacDA-1, and -RacDN-2 cells (Fig. 5). The expression levels of E-cadherin and β-catenin in sMDCK-Cdc42DA-2 and -Cdc42DN-6 cells were also similar to those in wild-type MDCK cells (data not shown). These results indicate that the changes in the staining intensity and the distribution of both E-cadherin and β-catenin are not due to the changes in the expression levels of both E-cadherin and β-catenin in sMDCK-RacDA-1 and -RacDN-2 cells.

ZO-1 is one of the structural proteins of tight junctions

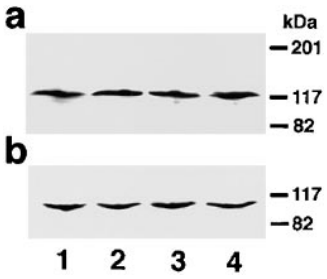

Figure 5. Expression levels of E-cadherin and β-catenin in sMDCK-RhoDA-5, -RacDA-1, and -RacDN-2 cells. Subconfluent MDCK cells were lysed, and protein samples were directly subjected to SDS-PAGE (10% polyacrylamide). The separated proteins were processed for immunoblotting with the C20820 anti–E-cadherin mAb (*a*) and the 5H10 anti–β-catenin mAb (*b*). Lane *1*, wild-type MDCK cells; lane *2*, sMDCK-RhoDA-5 cells; lane *3*, sMDCK-RacDA-1 cells; lane *4*, sMDCK-RacDN-2 cells. The prestained protein markers used were myosin (molecular weight, 201,000), β-galactosidase (molecular weight, 117,000), and bovine serum albumin (molecular weight, 82,000).

(Woods and Bryant, 1993) but is also partly colocalized with E-cadherin in MDCK cells (Howarth et al., 1994). We analyzed the localization of ZO-1 in sMDCK-RhoDA, -RacDA, -RacDN, -Cdc42DA, and -Cdc42DN cells. The staining patterns of ZO-1 in sMDCK-RhoDA-5, -RacDA-1, and -RacDN-2 cells were apparently indistinguishable from those in wild-type MDCK cells (Fig. 6). The staining patterns of ZO-1 in the other MDCK cell lines stably expressing V14RhoA, V12Rac1, or N17Rac1 were also similar to that in wild-type MDCK cells (data not shown). The staining patterns of ZO-1 in all the clones of sMDCK-Cdc42DA and -Cdc42DN were also similar to that in wild-type MDCK cells (data not shown). These results indicate that neither the Rho, the Rac, nor the Cdc42 subfamily affects the localization of ZO-1.

Electron Microscopic Analyses on the Cell–Cell Adhesion of sMDCK-RacDA and sMDCK-RacDN Cells

To understand the detailed changes in the localization of actin filaments, E-cadherin, and β-catenin in the MDCK cells stably expressing V12Rac1 or N17Rac1, we performed electron microscopic analyses on the morphology of the cell–cell adhesion and the localization of E-cadherin and β-catenin at the cell–cell adhesion sites in these cell lines. Wild-type MDCK cells tightly and linearly made contact with each other at the apical area of the lateral mem-

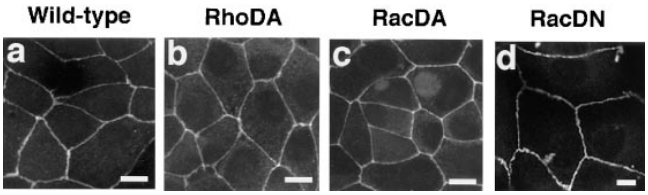

Figure 6. Localization of ZO-1 in sMDCK-RhoDA-5, -RacDA-1, and RacDN-2 cells. Wild-type MDCK cells (*a*), sMDCK-RhoDA-5 cells (*b*), sMDCK-RacDA-1 cells (*c*), and sMDCK-RacDN-2 cells (*d*) were stained with the anti–ZO-1 mAb and analyzed by confocal microscopy. Confocal images are shown at the junctional levels. Note that the scale in RacDN panels (*d*) is different from those in the other panels. The results shown are representative of three independent experiments. Bars, 10 μm.

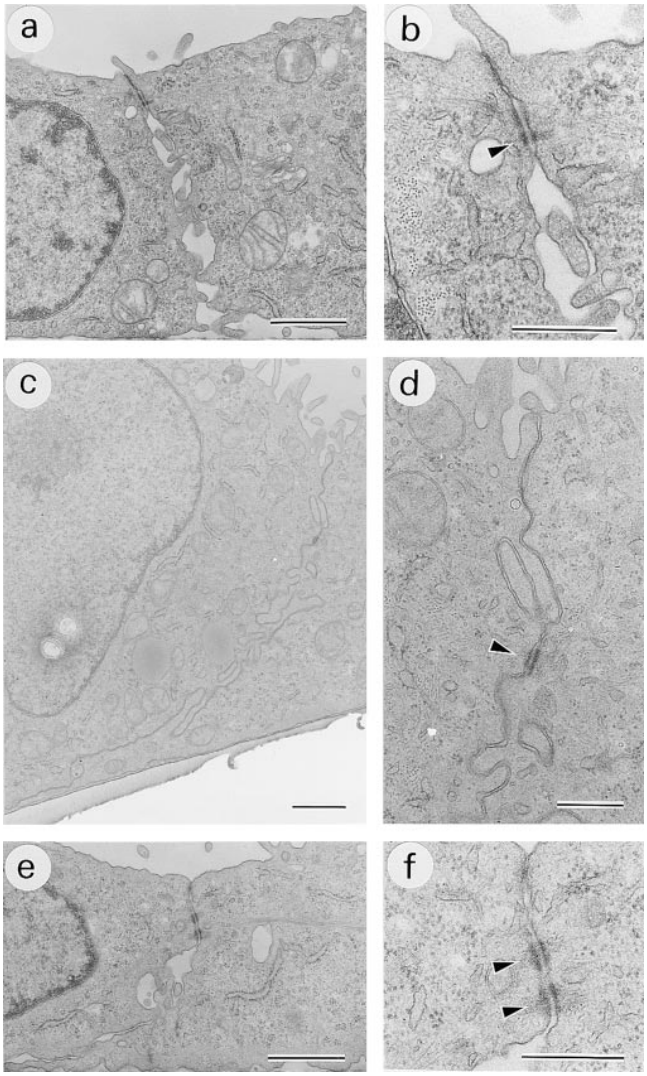

Figure 7. Electron microscopic analysis on the morphology of the cell–cell adhesion sites in wild-type MDCK, sMDCK-RacDA-1, and -RacDN-2 cells. Wild-type MDCK cells (*a* and *b*), sMDCK-RacDA-1 cells (*c* and *d*), and sMDCK-RacDN-2 cells (*e* and *f*) were fixed and processed for electron microscopy. *b*, *d*, and *f* show the cell–cell adhesion sites at higher magnifications of *a*, *c*, and *e*, respectively. Arrowheads indicate desmosomes. The results shown are representative of three independent experiments. Bars: (*a*, *c*, and *e*) 1 μm; (*b*, *d*, and *f*) 0.5 μm.

branes, whereas the cells loosely made contact at the other areas of the lateral membranes (Fig. 7 *a*). In contrast, sMDCK-RacDA-1 cells tightly made contact with each other throughout the lateral membranes (Fig. 7 *c*). No intercellular-free spaces were observed in these cells. Moreover, sMDCK-RacDA-1 cells were thicker and showed more markedly intermingled lateral membranes than wild-type MDCK cells. The morphology of the cell–cell adhesion in sMDCK-RacDN-2 cells resembled that in wild-type MDCK cells. sMDCK-RacDN-2 cells tightly made contact with each other at the apical area of the lateral membranes, whereas the cells loosely made contact at the basal side of the lateral membranes, although the cells were thinner than wild-type MDCK cells (Fig. 7 *e*). The desmosomes were apparently indistinguishable in all the cell

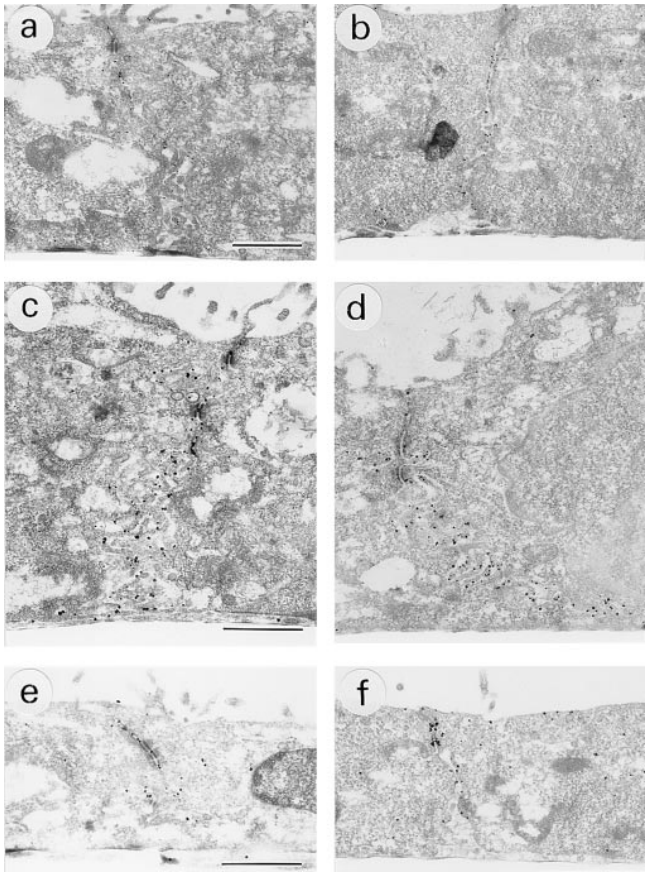

Figure 8. Immunoelectron microscopy analysis of the localization of E-cadherin and β-catenin at the cell–cell adhesion sites by immunoelectron microscopy in wild-type MDCK, sMDCK-RacDA-1, and -RacDN-2 cells. Wild-type MDCK cells (*a* and *b*), sMDCK-RacDA-1 cells (*c* and *d*), and sMDCK-RacDN-2 cells (*e* and *f*) were fixed and processed for immunoelectron microscopy using the ECCD-2 anti–E-cadherin mAb (*a*, *c*, and *e*) or the 5H10 anti–β-catenin mAb (*b*, *d*, and *f*). The results shown are representative of three independent experiments. Bars, 1 μm.

lines (Fig. 7, *b*, *d*, and *f*). These results indicate that the activation of the Rac subfamily strengthens the cell–cell adhesion without affecting the formation of the desmosomes.

Immunogold electron microscopic analysis showed that the gold particles of E-cadherin tended to be concentrated at the apical area from one fourth to one third of the lateral membranes, whereas they were sparsely observed at the basal side of the lateral membranes in wild-type MDCK and sMDCK-RacDN-2 cells (Fig. 8, *a* and *e*). The gold particles were observed densely throughout the lateral membranes in sMDCK-RacDA-1 cells (Fig. 8 *c*). The localization patterns of β-catenin were similar to those of E-cadherin (Fig. 8, *b*, *d*, and *f*). These results were consistent with those obtained by immunofluorescence microscopy and the detergent solubility assay.

Inhibition of the Formation of the Adherens and Tight Junctions by Microinjection of C3 into Wild-type MDCK Cells

The stable expression of V14RhoA in MDCK cells did not affect the cell–cell adhesion under the conditions where it

induced the formation of stress fibers and focal adhesions as described above. We attempted to obtain MDCK cell lines stably expressing a dominant negative mutant of RhoA, but we did not succeed in obtaining this type of transformant. Therefore, we investigated the effect of microinjection of C3, a *Clostridium botulinum* ADP-ribosyltransferase, into wild-type MDCK cells on the cell–cell adhesion. C3 ADP-ribosylates only the Rho subfamily of >60 members of the small G protein superfamily (Aktories et al., 1988; Kikuchi et al., 1988; Narumiya et al., 1988; Braun et al., 1989). C3 ADP-ribosylates Asn^{41} of the Rho subfamily, which is located at the putative effector domain, and the ADP-ribosylation impairs the functions of the Rho subfamily, presumably preventing the Rho subfamily from interacting with its effector protein (Sekine et al., 1989). We have previously shown that the most prominent and earliest effects of microinjection of C3 into wild-type MDCK cells were the disappearance of stress fibers and peripheral bundles and the inhibition of the localization of the ERM (Ezrin, Radixin, Moesin) family at peripheral bundles and vinculin at both focal adhesions and basal edges (Kotani et al., 1997). These effects of C3 were observed within 15 min after the microinjection. At 1 h after the microinjection, the actin filaments at the cell–cell adhesion sites started to disappear, and the microinjected cells separated with each other, although the actin filaments at the cell–cell adhesion sites between the microinjected and unmicroinjected cells were not apparently affected (Fig. 9, *a* and *d*). We then investigated the effect of microinjection of C3 into the cells on the localization of E-cadherin and ZO-1 at the cell–cell adhesion sites. At 30 min after the microinjection, the localization of both E-cadherin and ZO-1 at the cell–cell adhesion sites was not affected (data not shown), but at 1 h after the microinjection, the staining of both E-cadherin and ZO-1 at the cell–cell adhesion sites between the microinjected cells disappeared, whereas that between the microinjected and unmicroinjected cells was not apparently affected (Fig. 9, *b*, *c*, *e*, and *f*). These results indicate that the Rho subfamily is necessary for the maintenance of both the adherens and tight junctions.

We next investigated the effect of microinjection of C3 into wild-type MDCK cells on the Ca^{2+}-induced formation of both the adherens and tight junctions using Ca^{2+}-switch experiments. At 30 min before the Ca^{+}-switch experiments, the cells were microinjected with C3. The cells were then incubated in a low Ca^{2+} medium for 2 h, followed by the 2-h incubation in a normal Ca^{2+} medium. The incubation in a low Ca^{2+} medium induced disappearance of the staining of E-cadherin and ZO-1 at the cell–cell adhesion sites and the disruption of the cell–cell adhesion (data not shown), and the following incubation in a normal Ca^{2+} medium induced the localization of both E-cadherin and ZO-1 at the cell–cell adhesion sites and the formation of the cell–cell adhesion (Fig. 10, *a*, *b*, *d*, and *e*). The localization of both E-cadherin and ZO-1 at the cell–cell adhesion sites between the microinjected cells was inhibited, whereas that between the microinjected and unmicroinjected cells was not apparently inhibited (Fig. 10, *a*, *b*, *d*, and *e*). These results indicate that the Rho subfamily is also necessary for the Ca^{2+}-induced formation of both the adherens and tight junctions.

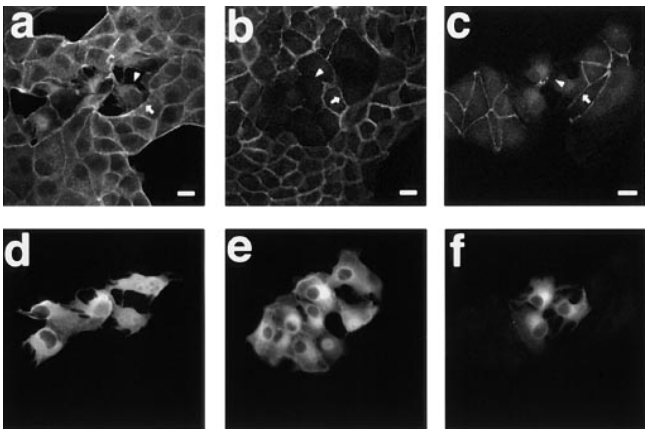

Figure 9. Disruption of the cell–cell adhesion in wild-type MDCK cells by microinjection of C3. Wild-type MDCK cells were fixed at 1 h after the microinjection with 40 μg/ml of C3 plus 5 mg/ml of rabbit IgG and stained with rhodamine-phalloidin (*a*), the ECCD-2 anti–E-cadherin mAb (*b*), or the anti–ZO-1 mAb (*c*), and analyzed by confocal microscopy. The microinjected cells are shown by the staining of microinjected rabbit IgG (*d–f*). Confocal images are shown at the junctional levels. The localization of the actin filaments, E-cadherin, and ZO-1 at the cell–cell adhesion sites was inhibited between the microinjected cells (*arrowheads*), whereas it was not inhibited between the microinjected and unmicroinjected cells (*arrows*). The results shown are representative of three independent experiments. Bars, 10 μm.

The intercellular binding of cadherins triggers the formation of adherens junctions, followed by the formation of tight junction in the Ca^{2+}-induced formation of cell–cell adhesion (Gonzalez-Mariscal et al., 1985, 1990; Contreras et al., 1992). However, activation of PKC induces the formation of the tight junction without the formation of the adherens junction in MDCK cells cultured in a low Ca^{+} medium (Balda et al., 1993). We investigated the effect of microinjection of C3 on the PKC-induced formation of the tight junction. At 30 min before the Ca^{2+} switch, the cells were microinjected with C3. The cells were then incubated in a low Ca^{2+} medium for 2 h, followed by the 1-h incubation in a low Ca^{2+} medium with 12-*O*-tetradecanoylphorbol-13-acetate (TPA). As shown previously (Balda et al., 1993), addition of TPA induced the localization of ZO-1 at the cell–cell adhesion sites (Fig. 10, *c* and *f*), whereas it did not induce the localization of E-cadherin at the cell–cell adhesion sites (data not shown). The TPA-induced localization of ZO-1 at the cell–cell adhesion sites between the microinjected cells was inhibited (Fig. 10, *c* and *f*), whereas that between the microinjected and unmicroinjected cells was not apparently inhibited (data not shown). These results indicate that the Rho subfamily is also necessary for the PKC-induced formation of the tight junction.

In contrast to the effect of C3 on wild-type MDCK cells, microinjection of C3 showed little effect on the localization of actin filaments and E-cadherin at the cell–cell adhesion sites in sMDCK-RacDA-1 cells (Fig. 11). The actin filaments at the cell–cell adhesion sites in sMDCK-RacDA-1 cells did not markedly change at 2 h after the microinjection, although a part of the actin filaments at the cell–cell adhesion sites was decreased, whereas the forma-

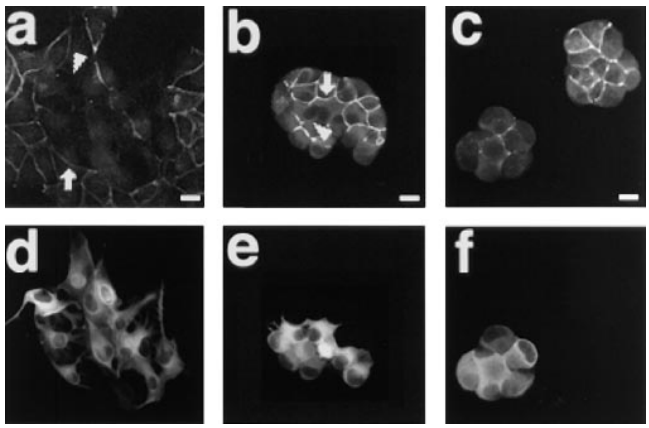

Figure 10. Inhibition of the formation of the cell–cell adhesion in wild-type MDCK cells by microinjection of C3. Wild-type MDCK cells cultured in normal Ca^{2+} DME were microinjected with 40 μg/ml of C3 plus 5 mg/ml of rabbit IgG. At 30 min after the microinjection the cells were transferred to low Ca^{2+} DME and further incubated for 2 h. The cells were then transferred to normal Ca^{2+} DME for 2 h (*a*, *b*, *d*, and *e*) or stimulated with 1×10^{-7} M TPA for 1 h (*c* and *f*). The cells were stained with the ECCD-2 anti–E-cadherin mAb (*a*) or the anti–ZO-1 mAb (*b* and *c*) and analyzed by confocal microscopy. The microinjected cells are shown by the staining of microinjected rabbit IgG (*d–f*). Confocal images are shown at the junctional levels. The localization of E-cadherin and ZO-1 at the cell–cell adhesion sites was inhibited between the microinjected cells (*arrowheads*), whereas it was not inhibited between the microinjected and unmicroinjected cells (*arrows*). The results shown are representative of three independent experiments. Bars, 10 μm.

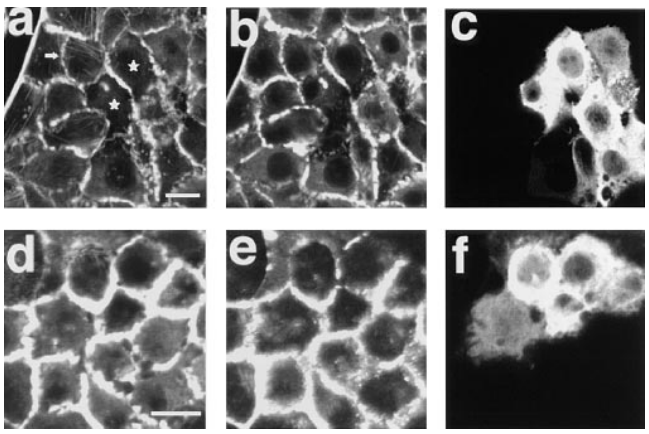

Figure 11. Inability of microinjection of C3 to disrupt the cell–cell adhesion in sMDCK-RacDA-1 cells. (*a–c*); sMDCK-RacDA-1 cells were fixed at 2 h after the microinjection with 40 μg/ml of C3 plus 5 mg/ml of rabbit IgG and stained with rhodamine-phalloidin (*a* and *b*) and analyzed by confocal microscopy. The microinjected cells are shown by the staining of microinjected rabbit IgG (*c*). (*a*) Basal level; (*b* and *c*) junctional levels. Stress fibers completely disappeared in the microinjected cells (*stars*), whereas the unmicroinjected cells possessed weak stress fibers (*arrow*). (*d–f*) sMDCK-RacDA-1 cells were fixed at 2 h after the microinjection with 40 μg/ml of C3 plus 5 mg/ml of rabbit IgG and stained with rhodamine-phalloidin (*d*) or the ECCD-2 anti–E-cadherin mAb (*e*) and analyzed by confocal microscopy. The microinjected cells are shown by the staining of microinjected rabbit IgG (*f*). Confocal images are shown at the junctional levels. The results shown are representative of three independent experiments. Bars, 10 μm.

tion of stress fibers was completely inhibited (Fig. 11, *a–d*, and *f*). The staining of E-cadherin at the cell–cell adhesion sites was not also apparently affected by the microinjection, although a part of E-cadherin at the cell–cell adhesion sites was decreased (Fig. 11, *e* and *f*). Even up to 4 h after the microinjection of C3 into sMDCK-RacDA-1 cells, the increased stainings of the actin filaments and E-cadherin were still observed at most of the cell–cell adhesion sites (data not shown). These results indicate that the Rho subfamily is not necessary for the Rac-induced increase in the localization of both the actin filaments and E-cadherin at the cell–cell adhesion sites.

Localization of RhoA, Rac1, and Cdc42 Mutants in MDCK Cell Lines Stably Expressing Various Rho, Rac, and Cdc42 Mutants

In the last set of experiments, we analyzed the localization of the *myc*-tagged proteins *myc*-V14RhoA, -V12Rac1, -N17Rac1, -V12Cdc42, and -N17Cdc42 and actin filaments in the stable transformant cell lines by double staining with the anti-*myc* mAb and rhodamine-phalloidin, respectively. Confocal microscopic images at the junctional levels showed that the significant staining was not observed in wild-type MDCK cells (Fig. 12, *a* and *e*). The weak and diffuse staining of V14RhoA was observed in sMDCK-RhoDA-5 cells (Fig. 12, *b* and *f*). However, V12Rac1 and N17Rac1 were highly concentrated at the cell–cell adhesion sites of sMDCK-RacDA-1 and -RacDN-2 cells, respectively, but the staining of V12Rac1 was stronger than that of N17Rac1 (Fig. 12, *c*, *d*, *g*, and *h*). The weak and diffuse stainings of V12Rac1 and N17Rac1 were also observed in the cytosol of both cell lines. At both the basal and apical levels, the weak and diffuse staining of V14RhoA was observed in sMDCK-RhoDA-5 cells (data not shown). The specific stainings of V12Rac1 and N17Rac1, except for the stainings at the cell–cell adhesion sites and the cytosol, were not observed at both the basal and apical levels in sMDCK-RacDA-1 and -RacDN-2 cells (data not shown). The essentially same results were obtained in the other cell lines stably expressing V14RhoA, V12Rac1, and N17Rac1 (data not shown). These results indicate that both the dominant active and negative mutants of Rac1 are localized mainly at the cell–cell adhesion sites, whereas the dominant active mutant of RhoA is localized mainly at the cytosol. However, because vinculin at the focal adhesions and the stress fibers markedly increased in sMDCK-RhoDA cells, compared with those of both wild-type MDCK, sMDCK-RacDA, and -RacDN cells (data not shown), the dominant active mutant of RhoA, which might be localized at the focal adhesions, might be masked by the cytosolic diffuse staining.

As to the localization of V12Cdc42, V12Cdc42 was highly concentrated at the cell–cell adhesion sites of sMDCK-Cdc42DA-2 cells as well as at the cytosol, although the localization of both the actin filaments, E-cadherin, and β-catenin was not apparently affected in sMDCK-Cdc42DA-2 cells as described above (data not shown). N17Cdc42 was localized mainly at the cytosol (data not shown).

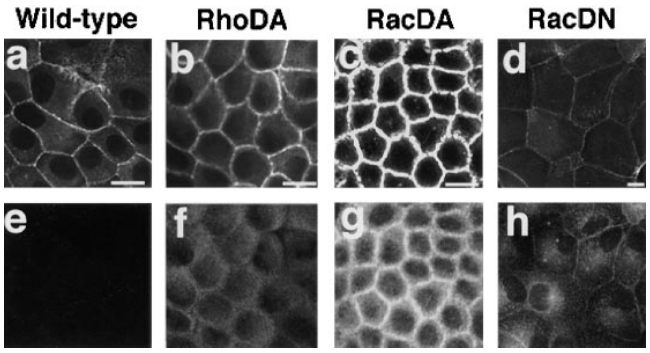

Figure 12. Localization of *myc*-tagged proteins in sMDCK-RhoDA-5, -RacDA-1, and -RacDN-2 cells. Wild-type MDCK cells (*a* and *e*), sMDCK-RhoDA-5 cells expressing *myc*-V14RhoA (*b* and *f*), sMDCK-RacDA-1 cells expressing *myc*-V12Rac1 (*c* and *g*), and sMDCK-RacDN-2 cells expressing *myc*-N17Rac1 (*d* and *h*) were double stained with rhodamine-phalloidin (*a–d*) and the 9E10 anti-*myc* mAb (*e–h*) and analyzed by confocal microscopy. Confocal images are shown at the junctional levels. The results shown are representative of three independent experiments. Bars, 10 μm.

Discussion

We have shown here by use of stable transformants of MDCK cells expressing various RhoA, Rac1, and Cdc42 mutants that the Rac subfamily regulates the cadherin-based cell–cell adhesion, but not the formation of the tight junction, that the Rho subfamily is necessary for both the cadherin-based cell–cell adhesion and the formation of the tight junction, and that the Cdc42 subfamily does not affect the cadherin-based cell–cell adhesion.

The expression of *myc*-V12Rac1 in sMDCK-RacDA was undetectable by immunoblotting with the anti-*myc* mAb using the cell lysates, whereas it was detected in the immunoprecipitated samples from the cell lysates. However, the localization of the actin filaments, E-cadherin, and β-catenin at the cell–cell adhesion sites markedly increased, suggesting that the dominant active mutant of Rac1 expressed to a small extent is able to induce the change in the actin cytoskeleton and adherens junctional proteins. The expression of *myc*-V14RhoA in sMDCK-RhoDA was also undetectable by immunoblotting with the anti-*myc* mAb using the cell lysates, whereas it was detected in the immunoprecipitated samples from the cell lysates, and the expression level of *myc*-V14RhoA was calculated to be less than one tenth of endogenous RhoA in sMDCK-RhoDA, when the expression level of endogenous RhoA was estimated by immunoblotting with the anti-RhoA polyclonal Ab. However, the formation of the stress fibers and the focal adhesions apparently increased in sMDCK-RhoDA, suggesting that the dominant active mutant of RhoA expressed to a small extent is enough to induce the change in the actin cytoskeleton. These results are consistent with the yeast results that activation of only a part of Rho1p is sufficient for the bud formation (Yamochi et al., 1994).

Immunohistochemical analysis revealed more intense staining of the actin filaments, E-cadherin, and β-catenin at the cell–cell adhesion sites and wider distribution of these proteins in sMDCK-RacDA cells than in wild-type MDCK cells, and conversely less intense staining and narrower distribution of these proteins in sMDCK-RacDN cells than in wild-type MDCK cells. The detergent solubility assay showed that the amount of detergent-insoluble E-cadherin increased in sMDCK-RacDA cells, whereas it decreased in sMDCK-RacDN cells. Electron microscopic analyses revealed that sMDCK-RacDA cells made tight contact with each other throughout the lateral membranes, whereas wild-type MDCK cells made contact tightly and linearly only at the apical side of the lateral membranes and that E-cadherin and β-catenin were localized densely throughout the lateral membranes of sMDCK-RacDA cells, whereas they were localized sparsely at the basal side of the lateral membranes of wild-type MDCK cells. These results clearly indicate that the E-cadherin–based cell–cell adhesion is markedly strengthened in sMDCK-RacDA cells. We furthermore attempted to perform cell aggregation assay using wild-type MDCK, sMDCK-RacDA, and -RacDN cells as described previously (Nagafuchi and Takeichi, 1988). However, we have not observed the significant difference in the activity of cell–cell adhesion in this assay (data not shown), suggesting that a dominant active or negative mutant of the Rac subfamily does not up regulate or down regulate, respectively, the activity of the E-cadherin–based cell–cell adhesion to the levels detectable by this cell aggregation assay. However, because it is generally difficult to measure correctly the activity of cell–cell adhesion of epithelial cells, which have not only cadherin-based cell–cell adhesion but also tight junction, by this cell aggregation assay, we reserve the conclusion on the effect of the Rac subfamily on this activity.

The mechanism by which the Rac subfamily regulates the E-cadherin–based cell–cell adhesion remains to be clarified, but one possibility is that it primarily induces the assembly of the actin filaments at the cell–cell adhesion sites, eventually leading to the assembly of E-cadherin and its related molecules, including α-, β-, and γ-catenins, p120 (Vestweber and Kemler, 1984; Peyrieras et al., 1985; Ozawa et al., 1989; Shibamoto et al., 1995), and unidentified molecules that link E-cadherin to actin filaments. Another possible mechanism is that the Rac subfamily directly regulates the function of E-cadherin or these related molecules through its downstream target molecule, eventually leading to the assembly of the actin filaments at the cell–cell adhesion sites.

The putative target molecules of the Rac subfamily were identified. They were $p65^{PAK}$, MLK2/3, MSE55, p60 S6kinase, POR-1, IQGAP1/2, WASP, and $p67^{phox}$ (for review see Tapon and Hall, 1997). The target molecule of the Rac subfamily that regulates the E-cadherin–based cell–cell adhesion is not known. Among the identified putative target molecules, IQGAP1/2 was localized at the cell–cell adhesion sites in MDCK cells (Hart et al., 1996; Kuroda et al., 1996). However, the localization of IQGAP1/2 was not apparently affected in sMDCK-RacDA and -RacDN cells, compared with that in wild-type MDCK cells (data not shown). Further studies are necessary to clarify the mode of action of the Rac subfamily.

We showed here by both confocal and electron microscopies that sMDCK-RacDA cells were thicker and sMDCK-RacDN cells thinner than the other cell lines. Moreover, the diameter of sMDCK-RacDN cells was ap-

parently larger than those of the other cell lines. The morphological changes in the cell shapes of sMDCK-RacDA and -RacDN cells may be due to alteration in the basolateral and/or the apical endo-exocytosis, because the Rac subfamily regulates endo-exocytosis (Komuro et al., 1996; Lamaze et al., 1996; O'Sullivan et al., 1996). Either the inhibition of endocytosis, the stimulation of exocytosis, or both may induce the enlargement of the plasma membrane, whereas either the stimulation of endocytosis, the inhibition of exocytosis, or both may induce the reduction of the plasma membrane.

The Rac subfamily regulates the formation of lamellipodia and membrane ruffles in many types of cultured cells, such as Swiss 3T3 and KB cells (Ridley et al., 1992; Nishiyama et al., 1994). Microinjection of the dominant active mutant of Rac1 induced membrane ruffling, whereas microinjection of the dominant negative mutant of Rac1 inhibited the growth factor-induced membrane rufflings in Swiss 3T3 cells (Ridley et al., 1992). However, in MDCK cells, microinjection of the dominant active mutant of Rac1 into this cell line did not induce membrane ruffling, whereas microinjection of the dominant negative mutant of Rac1 inhibited the hepatocyte growth factor–induced membrane ruffling (Ridley et al., 1995). In sMDCK-RacDA cells, the formation of lamellipodia or membrane ruffling did not increase, compared with that in wild-type MDCK cells, whereas the formation of lamellipodia and membrane ruffles apparently decreased in sMDCK-RacDN cells (data not shown). These results indicate that the Rac subfamily is necessary, but not sufficient, for the formation of lamellipodia and membrane ruffles in MDCK cells, whereas the Rac subfamily is sufficient for the formation of lamellipodia and membrane ruffles in Swiss 3T3 cells. These different actions of the Rac subfamily may be due to the difference of the cell types.

We previously showed that microinjection of the guanosine 5′-(3-*O*-thio) triphosphate-bound form of Rho into wild-type MDCK cells induced the formation of stress fibers and the localization of vinculin at the focal adhesions but did not induce the increased localization of the ERM family at the plasma membrane (Kotani et al., 1997). We showed here that the formation of stress fibers and focal adhesions markedly increased in sMDCK-RhoDA cells. However, the localization of the ERM family at the plasma membrane did not apparently increase in sMDCK-RhoDA cells, compared with that in wild-type MDCK cells (data not shown). These results are consistent with our previous results (Kotani et al., 1997). Moreover, we previously showed that microinjection of C3 into wild-type MDCK cells inhibited both the localization of the ERM family at the peripheral bundles and of vinculin at the basal edges of the colonies of the cells within 15 min after the microinjection (Kotani et al., 1997). We showed here that the later effect of microinjection of C3 into wild-type MDCK cells was disruption of the E-cadherin–based cell–cell adhesion and the tight junction. Furthermore, we showed here that microinjection of C3 also inhibited the Ca^{2+}-induced cell–cell adhesion and the TPA-induced formation of the tight junction. However, these effects of C3 were observed at the cell–cell adhesion between the microinjected cells, but not between the microinjected and unmicroinjected cells. Moreover, microinjection of C3 showed little effect on the increased localization of the actin filaments and E-cadherin at the cell–cell adhesion sites in sMDCK-RacDA cells. It is likely that the C3-induced loss of stress fibers, focal adhesions, and normal cell shape secondarily disrupts the cell–cell adhesion.

We showed here that both the dominant active mutant of Rac1, *myc*-V12Rac1, and the dominant negative mutant of Rac1, *myc*-N17Rac1, were localized at the cell–cell adhesion sites. *myc*-V12Rac1 may interact with the downstream target molecule at the cell–cell adhesion sites and exert its function there. Tiam1, a GDP/GTP exchange protein (GEP) for the Rac subfamily, was localized at the plasma membrane in fibroblasts (Michiels et al., 1995). N17Rac1 had higher affinity for GDP than for GTP and acted as a dominant negative mutant by binding to GEP (Ridley et al., 1992). Therefore, the localization of *myc*-N17Rac1 at the cell–cell adhesion sites may be due to its binding to GEP localized at the plasma membrane. In contrast to the localization of the Rac1 mutants, the dominant active mutant of RhoA, *myc*-V14RhoA, was localized mainly at the cytosol in sMDCK-RhoDA cells. The localization of *myc*-V14RhoA might be masked by the cytosolic diffuse staining, even if activated RhoA was translocated to the focal adhesions and induced the formation of the stress fibers and the focal adhesions through interaction with and activation of its downstream target molecule localized there. It is also possible that activated RhoA induced the formation of the stress fibers and the focal adhesions through interaction with and activation of its downstream target molecule localized at the cytosol.

During the review process of this manuscript, one report appeared, suggesting that both the Rho and Rac subfamilies are necessary for the E-cadherin–based cell–cell adhesion in human keratinocytes (Braga et al., 1997). Microinjection of C3, RacDN, or RacDA plus C3 inhibited the localization of E-cadherin at the cell–cell adhesion, whereas microinjection of neither RhoDA nor RacDA affected it. The effects of C3 and RacDN to inhibit the localization of E-cadherin at the cell–cell adhesion were observed at 25 min after the microinjection, and the inhibition of the E-cadherin–based cell–cell adhesion was observed between the microinjected cells and between the microinjected cells and unmicroinjected cells, suggesting that the Rho subfamily primarily regulates the E-cadherin–based cell–cell adhesion. As to the effect of RacDN and RhoDA, these results are consistent with our results, but as to the effect of C3 and RacDA, there are apparent discrepancies between these and our results. In our results, the time courses of C3 to inhibit the E-cadherin–based cell–cell adhesion in MDCK cells were apparently delayed, and the effect of C3 to inhibit the E-cadherin–based cell–cell adhesion in MDCK cells was observed only between the microinjected cells. Moreover, microinjection of C3 did not apparently inhibit the increased localization of E-cadherin in sMDCK-RacDA cells. Microinjection of RacDA did not affect the E-cadherin–based cell–cell adhesion in human keratinocytes, whereas sMDCK-RacDA cells showed increased localization of E-cadherin at cell–cell adhesion sites. In another previous report, the Rho subfamily regulated the formation of the tight junction and the perijunctional actin but did not affect the localization of E-cadherin or the actin filaments at the cell–cell adhesion sites in polarized intesti-

nal epithelial cells using DC3B, a chimeric toxin consisting of C3 and diphtheria toxin (Nusrat et al., 1995), whereas microinjection of C3 into wild-type MDCK cells inhibited the localization of both the actin filaments, E-cadherin, and ZO-1 at the cell–cell adhesion sites. The reasons for these discrepancies between these and our results are not known but may be due to the difference in assay conditions and/or difference of cell types.

We thank Dr. M. Takeichi (Kyoto University, Kyoto, Japan) for valuable discussions, and Dr. Sh. Tsukita for providing the anti–ZO-1 mAbs and valuable discussions. We thank Dr. W. Birchmeier for providing MDCK cells, Dr. A. Hall for the cDNAs of V12Rac1 and N17Rac1, Dr. K. Kaibuchi for anti-IQGAP pAb, Dr. P. Madaule for the cDNA of RhoA, Dr. A. Miyajima for the pSRαneo expression plasmid, Dr. S. Narumiya for C3, Dr. P. Polakis for the cDNA of Cdc42, and Dr. M.J. Wheelock for the anti–β-catenin mAb.

This investigation was supported by Grants-in-Aid for Scientific Research and for Cancer Research from the Ministry of Education, Science, Sports, and Culture, Japan (1995–1997), by Grants-in-Aid for Abnormalities in Hormone Receptor Mechanisms and for Aging and Health from the Ministry of Health and Welfare, Japan (1995–1997), and by grants from the Human Frontier Science Program (1995–1997) and the Uehara Memorial Foundation (1995–1996).

Received for publication 3 April 1997 and in revised form 4 September 1997.

References

Abo, A., E. Pick, A. Hall, N. Totty, C.G. Teahan, and A.W. Segal. 1991. Activation of the NADPH oxidase involves the small GTP-binding protein $p21^{rac1}$. *Nature.* 353:668–670.

Aktories, K., S. Rösener, U. Blaschke, and G.S. Chhatwal. 1988. Botulinum ADP-ribosyltransferase C3: purification of the enzyme and characterization of the ADP-ribosylation reaction in platelet membranes. *Eur. J. Biochem.* 172:445–450.

Ando, S., K. Kaibuchi, T. Sasaki, K. Hiraoka, T. Nishiyama, T. Mizuno, M. Asada, H. Nunoi, I. Matsuda, Y. Matsuura, et al. 1992. Post-translational processing of *rac* p21s is important both for their interaction with the GDP/GTP exchange proteins and for their activation of NADPH oxidase. *J. Biol. Chem.* 267:25709–25713.

Balda, M.S., L. Gonzalez-Mariscal, K. Matter, M. Cereijido, and J.M. Anderson. 1993. Assembly of the tight junction: the role of diacylglycerol. *J. Cell Biol.* 123:293–302.

Behrens, J., L. Vakaet, R. Friis, E. Winterhager, F. van Roy, M.M. Mareel, and W. Birchmeier. 1993. Loss of epithelial differentiation and gain of invasiveness correlate with tyrosine phosphorylation of the E-cadherin/β-catenin complex in cells transformed with a temperature-sensitive v-src gene. *J. Cell Biol.* 120:757–766.

Braga, V.M.M., L.M. Machesky, A. Hall, and N.A. Hotchin. 1997. The small GTPases Rho and Rac are required for the establishment of cadherin-dependent cell–cell contacts. *J. Cell Biol.* 137:1421–1431.

Braun, U., B. Habermann, I. Just, K. Aktories, and J. Vandekerckhove. 1989. Purification of the 22kDa protein substrate of botulinum ADP-ribosyltransferase C3 from porcine brain cytosol and its characterization as a GTP-binding protein highly homologous to the *rho* gene product. *FEBS Lett.* 243:70–76.

Chardin, P., P. Boquet, P. Madaule, M.R. Popoff, E.J. Rubin, and D.M. Gill. 1989. The mammalian G protein *rho*C is ADP-ribosylated by *Clostridium botulinum* exoenzyme C3 and affects actin microfilaments in Vero cells. *EMBO (Eur. Mol. Biol. Organ.) J.* 8:1087–1092.

Citi, S., H. Sabanay, R. Jakes, B. Geiger, and J. Kendrick-Jones. 1988. Cingulin, a new peripheral component of tight junctions. *Nature.* 333:272–276.

Contreras, R.G., J.H. Miller, M. Zamora, L. Gonzalez-Mariscal, and M. Cereijido. 1992. Interaction of calcium with the plasma membrane of epithelial (MDCK) cells during junction formation. *Am. J. Physiol.* 263:C313–C318.

Eaton, S., P. Auvinen, L. Luo, Y.N. Jan, and K. Simons. 1995. CDC42 and Rac1 control different actin-dependent processes in the *Drosophila* wing disc epithelium. *J. Cell Biol.* 131:151–164.

Furuse, M., T. Hirase, M. Itoh, A. Nagafuchi, S. Yonemura, Sa. Tsukita, and Sh. Tsukita. 1993. Occludin: a novel integral membrane protein localizing at tight junctions. *J. Cell Biol.* 123:1777–1788.

Furuse, M., M. Itoh, T. Hirase, A. Nagafuchi, S. Yonemura, Sa. Tsukita, and Sh. Tsukita. 1994. Direct association of occludin with ZO-1 and its possible involvement in the localization of occludin at tight junctions. *J. Cell Biol.* 127: 1617–1626.

Gonzalez-Mariscal, L., B. Chavez de Ramirez, and M. Cereijido. 1985. Tight junction formation in cultured epithelial cells (MDCK). *J. Membr. Biol.* 86: 113–125.

Gonzalez-Mariscal, L., R.G. Contreras, J.J. Bolivar, A. Ponce, B. Chavez de Ramirez, and M. Cereijido. 1990. Role of calcium in tight junction formation between epithelial cells. *Am. J. Physiol.* 259:C978–C986.

Hall, A. 1994. Small GTP-binding proteins and the regulation of the actin cytoskeleton. *Annu. Rev. Cell Biol.* 10:31–54.

Hamaguchi, M., N. Matsuyoshi, Y. Ohnishi, B. Gotoh, M. Takeichi, and Y. Nagai. 1993. $p60^{v\text{-}src}$ causes tyrosine phosphorylation and inactivation of the N-cadherin-catenin cell adhesion system. *EMBO (Eur. Mol. Biol. Organ.) J.* 12:307–314.

Hart, M.J., M.G. Callow, B. Souza, and P. Polakis. 1996. IQGAP1, a calmodulin-binding protein with a rasGAP-related domain, is a potential effector for cdc42Hs. *EMBO (Eur. Mol. Biol. Organ.) J.* 15:2997–3005.

Hirata, K., A. Kikuchi, T. Sasaki, S. Kuroda, K. Kaibuchi, Y. Matsuura, H. Seki, K. Saida, and Y. Takai. 1992. Involvement of *rho* p21 in the GTP-enhanced calcium ion sensitivity of smooth muscle contraction. *J. Biol. Chem.* 267: 8719–8722.

Howarth, A.G., K.L. Singer, and B.R. Stevenson. 1994. Analysis of the distribution and phosphorylation state of ZO-1 in MDCK and nonepithelial cells. *J. Membr. Biol.* 137:261–270.

Hülsken, J., W. Birchmeier, and J. Behrens. 1994. E-cadherin and APC compete for the interaction with β-catenin and the cytoskeleton. *J. Cell Biol.* 127: 2061–2069.

Jalink, K., E.J. van Corven, T. Hengeveld, N. Morii, S. Narumiya, and W.H. Moolenaar. 1994. Inhibition of lysophosphatidate- and thrombin-induced neurite retraction and neuronal cell rounding by ADP ribosylation of the small GTP-binding protein Rho. *J. Cell Biol.* 126:801–810.

Jesaitis, L.A., and D.A. Goodenough. 1994. Molecular characterization and tissue distribution of ZO-2, a tight junction protein homologous to ZO-1 and *Drosophila* disc-large tumor suppressor protein. *J. Cell Biol.* 124:949–961.

Keon, B.H., S. Schäfer, C. Kuhn, C. Grund, and W.W. Franke. 1996. Symplekin, a novel type of tight junction plaque protein. *J. Cell Biol.* 134:1003–1018.

Kikuchi, A., K. Yamamoto, T. Fujita, and Y. Takai. 1988. ADP-ribosylation of the bovine brain *rho* protein by botulinum toxin type C1. *J. Biol. Chem.* 263: 16303–16308.

Kishi, K., T. Sasaki, S. Kuroda, T. Itoh, and Y. Takai. 1993. Regulation of cytoplasmic division of *Xenopus* embryo by *rho* p21 and its inhibitory GDP/GTP exchange protein (*rho* GDI). *J. Cell Biol.* 120:1187–1195.

Knaus, U.G., P.G. Heyworth, T. Evans, J.T. Curnutte, and G.M. Bokoch. 1991. Regulation of phagocyte oxygen radical production by the GTP-binding protein rac2. *Science.* 254:1512–1515.

Komuro, R., T. Sasaki, K. Takaishi, S. Orita, and Y. Takai. 1996. Involvement of Rho and Rac Small G proteins and Rho GDI in Ca^{2+}-dependent exocytosis from PC12 cells. *Genes Cells.* 1:943–951.

Kotani, H., K. Takaishi, T. Sasaki, and Y. Takai. 1997. Rho regulates association of both the ERM family and vinculin with the plasma membrane in MDCK cells. *Oncogene.* 14:1705–1713.

Kozuma, R., S. Ahmed, A. Best, and L. Lim. 1995. The ras-related protein cdc42Hs and bradykinin promote formation of peripheral actin microspikes and filopodia in Swiss 3T3 fibroblasts. *Mol. Cell. Biol.* 15:1942–1952.

Kuroda, S., M. Fukata, K. Kobayashi, M. Nakafuku, N. Nomura, A. Iwamatsu, and K. Kaibuchi. 1996. Identification of IQGAP as a putative target for the small GTPases, Cdc42 and Rac1. *J. Biol. Chem.* 271:23363–23367.

Lamaze, C., T.-H. Chuang, L.J. Terlecky, G.M. Bokoch, and S.L. Schmid. 1996. Regulation of receptor-mediated endocytosis by Rho and Rac. *Nature.* 1996: 177–179.

Lang, P., L. Guizani, I. Vitté-Mony, R. Stancou, O. Dorseuil, G. Gacon, and J. Bertoglio. 1992. ADP-ribosylation of the *ras*-related, GTP-binding protein RhoA inhibits lymphocyte-mediated cytotoxicity. *J. Biol. Chem.* 267:11677–11680.

Luo, L., Y.J. Liao, L.Y. Jan, and Y.N. Jan. 1994. Distinct morphogenetic functions of similar small GTPases: *Drosophila* DRac1 is involved in axonal outgrowth and myoblast fusion. *Genes Dev.* 8:1787–1802.

Mabuchi, I., Y. Hamaguchi, H. Fujimoto, N. Morii, M. Mishima, and S. Narumiya. 1993. A rho-like protein is involved in the organization of the contractile ring in dividing sand dollar eggs. *Zygote.* 1:325–331.

Madara, J.L. 1988. Tight junction dynamics: is paracellular transport regulated? *Cell.* 53:497–498.

Matsuyoshi, N., M. Hamaguchi, S. Taniguchi, A. Nagafuchi, Sh. Tsukita, and M. Takeichi. 1992. Cadherin-mediated cell–cell adhesion is perturbed by v-src tyrosine phosphorylation in metastatic fibroblasts. *J. Cell Biol.* 118:703–714.

Michiels, F., G.G.M. Habets, J.C. Stam, R.A. van der Kammen, and J.G. Collard. 1995. A role for Rac in Tiam1-induced membrane ruffling and invasion. *Nature.* 375:338–340.

Miura, Y., A. Kikuchi, T. Musha, S. Kuroda, H. Yaku, T. Sasaki, and Y. Takai. 1993. Regulation of morphology by *rho* p21 and its inhibitory GDP/GTP exchange protein (*rho* GDI) in Swiss 3T3 cells. *J. Biol. Chem.* 268:510–515.

Mizoguchi, A., Y. Yano, H., Hamaguchi, H. Yanagida, C. Ide, A. Zahraoui, H. Shirataki, T. Sasaki, and Y. Takai. 1994. Localization of Rabphilin-3A on the synaptic vesicle. *Biochem. Biophys. Res. Commun.* 202:1235–1243.

Mizuno, T., K. Kaibuchi, S. Ando, T. Musha, K. Hiraoka, K. Takaishi, M. Asada, H. Nunoi, I. Matsuda, and Y. Takai. 1992. Regulation of the superoxide-generating NADPH oxidase by small GTP-binding protein and its stimulatory and inhibitory GDP/GTP exchange proteins. *J. Biol. Chem.* 267: 10215–10218.

Morii, N., T. Teru-uchi, T. Tominaga, N. Kumagai, S. Kozaki, F. Ushikubi, and S. Narumiya. 1992. A *rho* gene product in human blood platelets. II. Effects of the ADP-ribosylation by botulinum C3 ADP-ribosyltransferase on platelet aggregation. *J. Biol. Chem.* 267:20921–20926.

Nagafuchi, A., and M. Takeichi. 1988. Cell binding function of E-cadherin is regulated by the cytoplasmic domain. *EMBO (Eur. Mol. Biol. Organ.) J.* 12: 3679–3684.

Narumiya, S., A. Sekine, and M. Fujiwara. 1988. Substrate for botulinum ADP-ribosyltransferase, Gb, has an amino acid sequence homologous to a putative *rho* gene product. *J. Biol. Chem.* 263:17255–17257.

Nishiyama, T., T. Sasaki, K. Takaishi, M. Kato, H. Yaku, K. Araki, Y. Matsuura, and Y. Takai. 1994. *rac* p21 is involved in insulin-induced membrane ruffling and *rho* p21 is involved in hepatocyte growth factor- and 12-*O*-tetradecanoyl-phorbol-13-acetate (TPA)-induced membrane ruffling in KB cells. *Mol. Cell. Biol.* 14:2447–2456.

Nobes, C.D., and A. Hall. 1995. Rho, rac, and cdc42 GTPases regulate the assembly of multimolecular focal complexes associated with actin stress fibers, lamellipodia and filopodia. *Cell.* 81:53–62.

Nusrat, A., M. Giry, J.R. Turner, S.P. Colgan, C.A. Parkos, D. Carnes, E. Lemichez, P. Boquet, and J.L. Madara. 1995. Rho protein regulates tight junctions and perijunctional actin organization in polarized epithelia. *Proc. Natl. Acad. Sci. USA.* 92:10629–10633.

O'Sullivan, A.J., A.M. Brown, H.N.M. Freeman, and B.D. Gomperts. 1996. Purification and identification of foad-II, a cytosolic protein that regulates secretion in streptolysin-O permeabilized mast cells, as a rac/rho GDI complex. *Mol. Biol. Cell.* 7:397–408.

Ozawa, M., H. Baribault, and R. Kemler. 1989. The cytoplasmic domain of the cell adhesion molecule uvomorulin associates with three independent proteins structurally related in different species. *EMBO (Eur. Mol. Biol. Organ.) J.* 8:1711–1717.

Paterson, H.F., A.J. Self, M.D. Garrett, I. Just, K. Aktories, and A. Hall. 1990. Microinjection of recombinant $p21^{rho}$ induces rapid changes in cell morphology. *J. Cell Biol.* 111:1001–1007.

Peyrieras, N., D. Louvard, and F. Jacob. 1985. Characterization of antigens recognized by monoclonal and polyclonal antibodies directed against uvomorulin. *Proc. Natl. Acad. Sci. USA.* 82:8067–8071.

Ridley, A.J., and A. Hall. 1992. The small GTP-binding protein rho regulates the assembly of focal adhesions and actin stress fibers in response to growth factors. *Cell.* 70:389–399.

Ridley, A.J., and A. Hall. 1994. Signal transduction pathways regulating Rho-mediated stress fibre formation: requirement for a tyrosine kinase. *EMBO (Eur. Mol. Biol. Organ.) J.* 13:2600–2610.

Ridley, A.J., H.F. Paterson, C.L. Johnstone, D. Diekmann, and A. Hall. 1992. The small GTP-binding protein rac regulates growth factor-induced membrane ruffling. *Cell.* 70:401–410.

Ridley, A.J., P.M. Comoglio, and A. Hall. 1995. Regulation of scatter factor/hepatocyte growth factor responses by Ras, Rac, and Rho in MDCK cells. *Mol. Cell. Biol.* 15:1110–1122.

Rubin, E.J., D.M. Gill, P. Boquet, and M.R. Popoff. 1988. Functional modification of a 21-kilodalton G protein when ADP-ribosylated by exoenzyme C3 of *Clostridium botulinum. Mol. Cell. Biol.* 8:418–426.

Schmalzing, G., H.-P. Richter, A. Hansen, W. Schwarz, I. Just, and K. Aktories. 1995. Involvement of the GTP binding protein Rho in constitutive endocytosis in *Xenopus laevis* oocytes. *J. Cell Biol.* 130:1319–1332.

Sekine, A., M. Fujiwara, and S. Narumiya. 1989. Asparagine residue in the *rho* gene product is the modification site for botulinum ADP-ribosyltransferase. *J. Biol. Chem.* 264:8602–8605.

Self, A.J., H.F. Paterson, and A. Hall. 1993. Different structural organization of Ras and Rho effector domains. *Oncogene.* 8:655–661.

Shibamoto, S., M. Hayakawa, K. Takeuchi, T. Hori, K. Miyazawa, N. Kitamura, K.R. Johnson, M.J. Wheelock, N. Matsuyoshi, M. Takeichi, et al. 1995. Association of p120, a tyrosine kinase substrate, with E-cadherin/catenin complexes. *J. Cell Biol.* 128:949–957.

Stasia, M.-J., A. Jouan, N. Bourmeyster, P. Boquet, and P.V. Vignais. 1991. ADP-ribosylation of a small size GTP-binding protein in bovine neutrophils by the C3 exoenzyme of *Clostridium botulinum* and effect on the cell motility. *Biochem. Biophys. Res. Commun.* 180:615–622.

Stowers, L., D. Yelon, L.J. Berg, and J. Chant. 1995. Regulation of the polarization of T cells toward antigen-presenting cells by Ras-related GTPase CDC42. *Proc. Natl. Acad. Sci. USA.* 92:5027–5031.

Takai, Y., T. Sasaki, K. Tanaka, and H. Nakanishi. 1995. Rho as a regulator of the cytoskeleton. *Trends Biochem. Sci.* 20:227–231.

Takeichi, M. 1977. Functional correlation between cell adhesive properties and some surface proteins. *J. Cell Biol.* 75:464–474.

Takeichi, M. 1995. Morphogenetic roles of classic cadherins. *Curr. Opin. Cell Biol.* 7:619–627.

Takaishi, K., A. Kikuchi, S. Kuroda, K. Kotani, T. Sasaki, and Y. Takai. 1993. Involvement of *rho* p21 and its inhibitory GDP/GTP exchange protein (*rho* GDI) in cell motility. *Mol. Cell. Biol.* 13:72–79.

Takaishi, K., T. Sasaki, M. Kato, W. Yamochi, S. Kuroda, T. Nakamura, M. Takeichi, and Y. Takai. 1994. Involvement of *rho* p21 small GTP-binding protein and its regulator in the HGF-induced cell motility. *Oncogene.* 9:273–279.

Takaishi, K., T. Sasaki, T. Kameyama, Sa. Tsukita, Sh. Tsukita, and Y. Takai. 1995. Translocation of activated *Rho* from the cytoplasm to membrane ruffling area, cell–cell adhesion sites and cleavage furrows. *Oncogene.* 11:39–48.

Tapon, N., and A. Hall. 1997. Rho, Rac and Cdc42 GTPases regulate the organization of the actin cytoskeleton. *Curr. Opin. Cell Biol.* 9:86–92.

Tominaga, T., K. Sugie, M. Hirata, N. Morii, J. Fukata, A. Uchida, H. Imura, and S. Narumiya. 1993. Inhibition of PMA-induced, LFA-1–dependent lymphocyte aggregation by ADP ribosylation of the small molecular weight GTP binding protein, *rho. J. Cell Biol.* 120:1529–1537.

Tsukita, Sh., Sa. Tsukita, A. Nagafuchi, and S. Yonemura. 1992. Molecular linkage between cadherins and actin filaments in cell–cell adherens junctions. *Curr. Opin. Cell Biol.* 4:834–839.

Tsukita, Sh., M. Itoh, A. Nagafuchi, S. Yonemura, and Sa. Tsukita. 1993. Submembranous junctional plaque proteins include potential tumor suppressor molecules. *J. Cell Biol.* 123:1049–1053.

Vestweber, D., and R. Kemler. 1984. Some structural and functional aspects of the cell adhesion molecule uvomorulin. *Cell Differ.* 15:269–273.

Woods, D.F., and P.J. Bryant. 1993. ZO-1, DlgA and PSD-95/SAP90: homologous proteins in tight, septate and synaptic cell junctions. *Mech. Dev.* 44:85–89.

Yamochi, W., K. Tanaka, H. Nonaka, A. Maeda, T. Musha, and Y. Takai. 1994. Growth site localization of RHO1 small GTP-binding protein and its involvement in bud formation in *Saccharomyces cerevisiae. J. Cell Biol.* 125: 1077–1093.

Zahraoui, A., G. Joberty, M. Arpin, J.J. Fontaine, R. Hellio, A. Tavitian, and D. Louvard. 1994. A small rab GTPase is distributed in cytoplasmic vesicles in nonpolarized cells but colocalized with the tight junction marker ZO-1 in polarized epithelial cells. *J. Cell Biol.* 124:101–115.

Zhong, Y., T. Saitoh, T. Minase, N. Sawada, Y. Enomoto, and M. Mori. 1993. Monoclonal antibody 7H6 reacts with a novel tight junction-associated protein distinct from ZO-1, cingulin, and ZO-2. *J. Cell Biol.* 120:477–483.